Thin Porous Alumina Sheets as Supports for Stabilizing Gold Nanoparticles

Jie Wang,[†] An-Hui Lu,[†] Mingrun Li,[‡] Weiping Zhang,[†] Yong-Sheng Chen,[§] Dong-Xu Tian,[†] and Wen-Cui Li[†,*]

[†]State Key Laboratory of Fine Chemicals, School of Chemical Engineering, Dalian University of Technology, Dalian 116024, People's Republic of China, [‡]State Key Laboratory of Catalysis, Dalian Institute of Chemical Physics, Chinese Academy of Sciences, Dalian 116023, People's Republic of China, and [§]EMS Energy Institute, and John and Willie Leone Family Department of Energy and Mineral Engineering, Pennsylvania State University, University Park, Pennsylvania 16802, United States

ABSTRACT Thin porous alumina sheets have been synthesized using a lysine-assisted hydrothermal approach resulting in an extraordinary catalyst support that can stabilize Au nanoparticles at annealing temperatures up to 900 °C. Remarkably, the unique architecture of such an alumina with thin sheets (average thickness ~15 nm and length 680 nm) and rough surface is beneficial to prevent gold nanoparticles from sintering. HRTEM observations clearly showed that the epitaxial growth between Au nanoparticles and alumina support was due to strong interfacial interactions, further explaining the high sinter-stability of the obtained Au/Al_2O_3 catalyst. Consequently, despite calcination at 700 °C, the catalyst maintains its gold nanoparticles of size predominantly 2 ± 0.8 nm. Surprisingly, catalyst annealed at 900 °C retained the highly dispersed small gold nanoparticles. It was also observed that a few gold particles (6−25 nm) were encapsulated by an alumina layer (thickness less than 1 nm) to minimize the surface energy, revealing a surface restructuring of the gold/support interface. As a typical and size-dependent reaction, CO oxidation is used to evaluate the performance of Au/Al_2O_3 catalysts. The results obtained demonstrated Au/Al_2O_3 catalyst calcined at 700 °C exhibited excellent activity with a complete CO conversion at ~30 °C ($T_{100\%}$ = 30 °C), and even after calcination at 900 °C, the catalyst still achieved its $T_{50\%}$ at 158 °C. In sharp contrast, Au catalyst prepared using conventional alumina support shows almost no activity under the same preparation and catalytic test conditions.

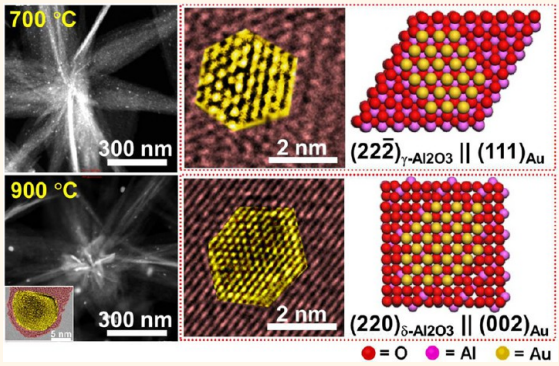

KEYWORDS: porous alumina sheet · gold nanoparticles · strong interfacial interaction · high temperature · epitaxial growth

In recent years, one of the most challenging topics in materials chemistry and catalysis has been the synthesis of hierarchical catalyst supports with controlled morphologies and nanoarchitecture, and in particular with the ability of being able to stabilize noble metal particles (NMPs) against sintering. It is known that particle aggregation, owing to the increased mobility of particles at high temperatures, often causes catalyst deactivation, limiting their use.[1−4]

To prevent this serious problem, a feasible and sophisticated solution is to confine NMPs in microenvironments. In general, two types of support, *i.e.*, mesostructures and hollow cages, are utilized for the stabilization of NMPs, such as Au and Ag in mesoporous materials,[5−8] Fe in CNTs,[9] or encapsulation of NMPs in a robust cage structure, $Au@ZrO_2$,[10] $Au@TiO_2$,[11] $Au@SiO_2$,[12] $Au@SnO_2$,[13] $Pt@mSiO_2$,[14] Pt@hmC,[15] or Pt@CoO.[16] These well-controlled structures can be regarded as model systems for the fundamental understanding of catalytic effects. However, the developed synthesis methods tend to be rather complicated, particularly for the fabrication of nanocage structures involving multiple steps. Thus, there is considerable interest to develop an alternative, simple, and effective strategy for the synthesis of new structured support materials with the capability of immobilizing and stabilizing NMPs against sintering.

The catalyst support needs to fulfill the following requirements: it should be thermally stable to maintain the morphology of the catalyst; it should contain a sufficient

* Address correspondence to wencuili@dlut.edu.cn.

Received for review January 8, 2013 and accepted May 19, 2013.

Published online May 20, 2013
10.1021/nn401446p

amount of small mesopores or roughness that can immobilize the metal nanoparticles in a size matching manner; and it should have an open structure to allow easy access to reacting agents. Following this line, porous alumina is one of the most widely used industrial substances with the essential properties of high surface area and good mechanical, chemical, and especially thermal stability. To date, several synthesis methods, such as soft-templating[17] and hard-templating methods,[18,19] have been developed to fabricate porous aluminum oxides. These oxides are some of the most widely studied catalyst supports in both industry and academic research. However, until now, it has been difficult to find a successful method using porous alumina to stabilize noble metals, particularly Au nanoparticles, against sintering at temperatures exceeding 700 °C. Thus, the challenge remains to develop a simple and effective strategy to overcome this barrier and to produce a porous aluminum oxide with the above-mentioned architecture and properties.

Herein, our strategy is to synthesize Al_2O_3 with 3D configuration composed of thin sheets giving an open structure and rough surface so as to immobilize Au nanoparticles and provide some thermal stability. This designed structure would ideally realize the spatial stabilization of supported Au, and the separated alumina sheets can prevent the contact of Au nanoparticles. We have found that when using lysine as a "shape-inducing" reagent together with urea as precipitating agent and $Al(NO_3)_3 \cdot 9H_2O$ as precursor, thin porous alumina sheets can be consequently obtained through a hydrothermal synthesis. To test the capability of such an alumina to stabilize nanosized noble metal particles, Au nanoparticles with a relatively low Tammamn temperature of ~395 °C (particles 2 nm in diameter would have a melting point of 300 °C) have been selected as the target. It is known that the CO oxidation reaction is sensitive to the size of the Au nanoparticles (Au nanoparticles with sizes below 5 nm exhibit excellent catalytic activity),[20−22] and thus we chose CO oxidation as the model reaction to evaluate the activity of the supported catalysts. The results are surprising in that although the Au/Al_2O_3 catalyst was calcined at 700 °C, the gold nanoparticle size was almost unchanged at 2 ± 0.8 nm, and complete conversion of the 1% CO was achieved at ~30 °C. To the best of our knowledge, such a result has never been published in the literature. This thus provides an alternative solution for the synthesis of a catalyst support that can effectively stabilize nanosized noble metals, besides the conventional strategies using core−shell (or cage) structures and mesoporous solids as the confined environments.

RESULTS AND DISCUSSION

Properties of Thin Porous Alumina Sheets. Boehmite (γ-AlO(OH)) is an aluminum oxyhydroxide that can be converted to many different forms of alumina through thermal annealing. Hence, the control of the size and shape of the boehmite nanostructures is key to improving the properties and thus potential applications of the resultant alumina. Recently, amino acids have been proven as powerful "shape-inducing" reagents to prepare nanomaterials with various morphologies.[23−27] In the current study, using lysine as a "shape-inducing" reagent together with urea as precipitating agent and $Al(NO_3)_3 \cdot 9H_2O$ as precursor, thin porous alumina sheets were produced through a hydrothermal synthesis (Figure 1a). Figure 1b shows a rough surface of γ-Al_2O_3 sheets. In addition, the intermediate species at different intervals during the hydrothermal synthesis were characterized by means of SEM, FTIR, and XRD techniques (Figure S1). It can be seen that, with the increase in hydrothermal period, the morphologies of the obtained samples transform from irregular to fiber to thin sheets and finally to star-shaped sheets. The possible structural evolution mechanism is discussed in the Supporting Information. Notably, the simultaneous use of lysine and urea during the synthesis is an indispensable factor for achieving such star-shaped solid materials.

To explore the thermal decomposition behavior of the hydrothermal product, sample Al_2O_3-1-hydro was characterized by TG/DSC-MS under air, with a heating rate of 10 °C min^{-1}. As seen in Figure 1c, the exhaust gases were monitored by an online mass spectrometer (MS). On the basis of the TG-DSC curves, we deduce that AlO(OH) is the primary component of Al_2O_3-1-hydro ($2AlO(OH) \rightarrow Al_2O_3 + H_2O$ with a theoretical weight loss value of ~15%).[28,29] The TG curve shows a sharp weight loss of ~17% before 450 °C, mainly corresponding to the release of adsorbed water and the decomposition of lysine adsorbed on the surfaces. In this stage, boehmite is converted to γ-alumina during the subsequent heating as the elimination of H_2O between boehmite layers takes place. The TG curve between 450 and 900 °C shows a small gradual loss of ~3%. The DSC curve of Al_2O_3-1-hydro displays a broad exothermic peak up to 350 °C, which can be attributed to the phase conversion. In addition, the main peak position of H_2O ($m/z = 18$) and NH_3 ($m/z = 17$) was produced at 180 and 450 °C during the calcination of Al_2O_3-1-hydro. Fragments of CO_2 ($m/z = 44$) are mainly detected at 180, 360, and 530 °C, which are derived from lysine and urea. The TG/DSC-MS curves indicate that after 500 °C the hydroxyl groups and amine groups have been eliminated to a great extent. This is further confirmed by the XPS analysis shown in Figure S2a, where there are no detectable nitrogen species on the surfaces of the Al_2O_3-1, although the surface C content is 2.1 wt %. On the basis of the above, we thus selected 500 °C as the annealing temperature.

Generally, *via* the calcination of aluminum hydroxide (boehmite, AlO(OH)), a sequential transformation of alumina can be achieved over the temperature

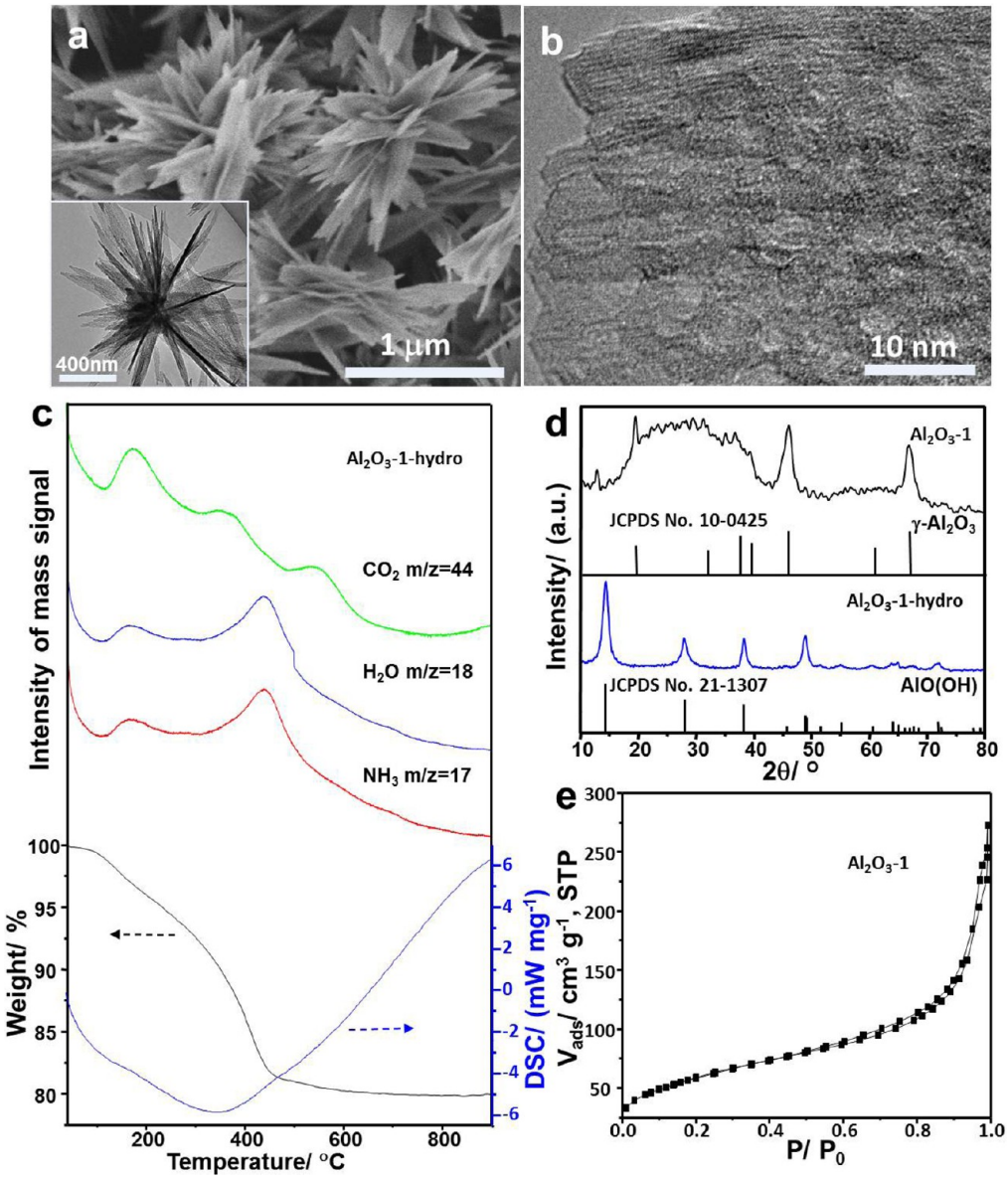

Figure 1. (a) SEM (inset is the corresponding TEM image) and (b) TEM images of Al_2O_3-1. (c) TG/DSC-MS curves of sample Al_2O_3-1-hydro. (d) XRD patterns of Al_2O_3-1 and Al_2O_3-1-hydro. (e) N_2 sorption isotherm of Al_2O_3-1.

range 450−750 °C (γ-Al_2O_3), 800−1000 °C (δ-Al_2O_3), and 1000−1200 °C (θ-Al_2O_3) and, finally, above 1200 °C (α-Al_2O_3).[30] Based on the XRD pattern in Figure 1d, the AlO(OH) phase (JCPDS No. 21-1307) with a high degree of crystallinity was obtained after hydrothermal treatment for 24 h. Following annealing at 500 °C, γ-Al_2O_3 (JCPDS No. 10-0425) is formed. The nitrogen sorption isotherm (Figure 1e) of Al_2O_3-1 is essentially a pseudo-type II, showing interparticle capillary condensation. Elemental analysis of the sample Al_2O_3-1 indicates that the amount of N is negligible and confirms the purity of the calcined Al_2O_3-1 support. Similarly, the XPS results and the FTIR spectrum (Figure S2) of the calcined Al_2O_3-1 show that almost no nitrogen species derived from lysine and urea can be detected on the surface of Al_2O_3-1. The bands at 3445 and 1639 cm^{-1} are ascribed to the stretching vibrations of OH groups in the hydroxide structure and physically adsorbed water,[31−33] while the weak characteristic peaks at 1528 may be from carbonate species.[34−36] The band at 1385 cm^{-1} is attributed to water molecules coordinated to Lewis acid sites in γ-Al_2O_3.[37,38]

Gold Nanoparticles Supported on Thin Porous Alumina Sheets. Using the thin porous γ-Al_2O_3 sheets as the catalytic support, Au nanoparticles were introduced using the deposition−precipitation method, followed by annealing in air at 700 and 900 °C. Due to the quantum-size effect, Au nanoparticles with relatively lower Tammann temperature (395 °C; particles 2 nm in diameter would have a melting point of 300 °C) are easily sintered at elevated temperatures.[4,39] Thus to our surprise, the Au nanoparticles on our novel alumina support exhibited an excellent sinter stability during a high-temperature treatment up to 900 °C.

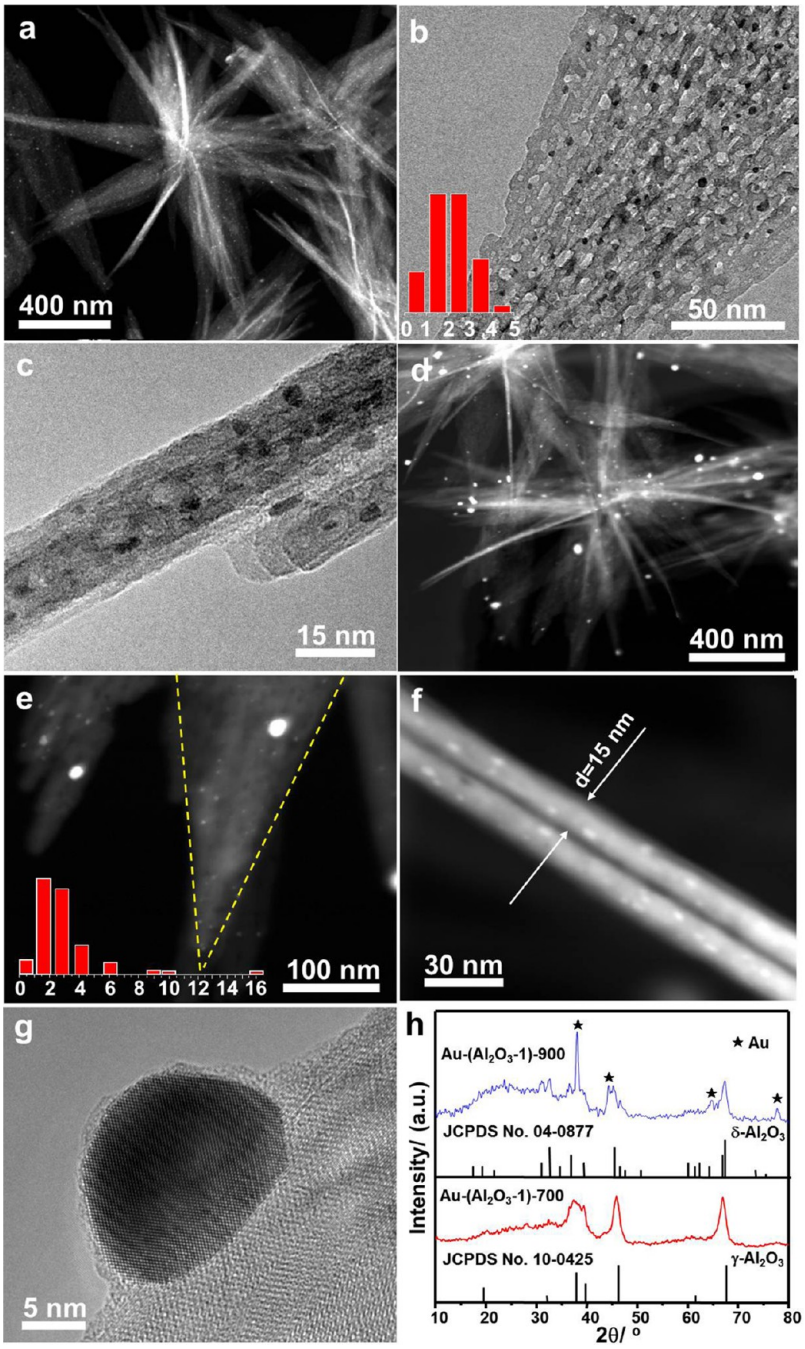

Figure 2. STEM and TEM images of gold catalyst (a−c) Au-(Al_2O_3-1)-700 and (d−g) Au-(Al_2O_3-1)-900. (h) The corresponding XRD patterns.

As clearly shown in Figure 2a,b and Figure S3, Au nanoparticles predominantly 2 ± 0.8 nm in size are highly dispersed on the Au-(Al_2O_3-1)-700. Figure 2c shows a high-resolution transmission electron microscopy (HRTEM) image of a thin sheet (~15 nm in thickness), on which multitudes of tiny Au nanoparticles are highly distributed. The elongated shape of the Au particles may stem from the strong interfacial interaction of Au−alumina, and thus Au particles may adapt themselves to the porous nature of the alumina support. Even after annealing at 900 °C, a significant amount of small gold nanoparticles (average size 2−4 nm) still exist in the Au-(Al_2O_3-1)-900 catalyst (Figure 2d,e and Figures S4, S5), although a small number of larger gold nanoparticles up to 25 nm can also be observed. In Figure 2f one can observe two thin sheets of alumina where the thickness of each flake is *ca.* 15 nm. A number of well-distributed Au nanoparticles were anchored on the alumina support. In Figure 2g, a closer look at one Au particle reveals that it was encapsulated by an uneven alumina layer with a thickness less than 1 nm. This reveals a surface restructuring of the gold/support interfaces. Although Al_2O_3 is generally regarded as a nonreducible support

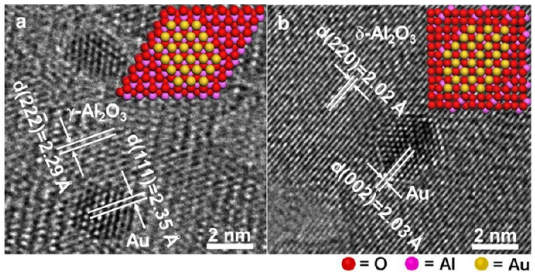

Figure 3. HRTEM images (inset is the corresponding schematic drawings) of gold catalysts (a) Au-(Al_2O_3-1)-700 and (b) Au-(Al_2O_3-1)-900.

in gold catalysts,[40] reported here is the first observation that such a typical inert support, Al_2O_3, has encapsulated Au on the surface, indicating the existence of a strong metal support interaction (SMSI) between gold and the alumina support. A similar phenomenon was recently observed for Au/ZnO catalysts calcined at 300 °C.[41] It is known that a SMSI occurs when the group VIII metals Fe, Ni, Rh, Pt, Pd, and Ir are supported on certain oxides (TiO_x, TaO_x, CeO_x, and NbO_x), and the activity and selectivity are mainly dependent on the strong interaction between the active metal and defects of those reducible oxides.[42] As seen in Figure 2h, the XRD pattern of gold catalyst Au-(Al_2O_3-1)-700 exhibits diffraction peaks of γ-Al_2O_3 (JCPDS No. 10-0425), with no detectable peaks assigned to Au, which suggests the deposited Au particles retain their small size and high dispersion. The XRD pattern of the Au-(Al_2O_3-1)-900 shows diffraction peaks of δ-Al_2O_3 (JCPDS No. 04-0877), together with some characteristic peaks of Au nanoparticles. The determined crystallite size of the Au nanoparticles is approximately 23 nm based on the Scherrer equation, which is consistent with TEM observations. It is important to note that the XRD analysis always gives the size information of the larger particles.

Furthermore, the interactions between Au nanoparticles and alumina are clearly evidenced through HRTEM (Figure 3). In the case of Au-(Al_2O_3-1)-700, the crystal lattice of Au(111) is measured as 2.35 Å (Figure 3a), while the value of γ-Al_2O_3 ($22\bar{2}$) is 2.29 Å. This indicates that the Au nanoparticles are mainly attached epitaxially on the γ-Al_2O_3 through the most densely packed (111) plane, despite a ~2.5% mismatch between the lattice spacing of Au(111) and γ-Al_2O_3-($22\bar{2}$).[4,22] To reduce the structural strain, lattice mismatch is known to play a significant role in the epitaxial growth of heterogeneous structures.[43,44] In regard to Au-(Al_2O_3-1)-900, the lattice distance of Au(002) is approximately 2.02 Å, which is in good agreement with the value of δ-Al_2O_3(220) facet (2.03 Å) (Figure 3b). Thus, HRTEM observations have confirmed that the interface between the Au nanoparticles and alumina support is coherent. As is well known, interphase boundaries can be termed as coherent, semicoherent, or incoherent depending on the nature of match between atoms across the interface, and the interfacial energy increases in the order of coherent, semicoherent, and incoherent interfaces.[45] Therefore, this further supports the epitaxial growth relationship between Au(002) and δ-Al_2O_3(220) and explains the high sinter stability of the obtained Au/Al_2O_3 catalysts.

CO Oxidation. As a typical and size-dependent reaction, CO oxidation has been chosen to evaluate the activity and sinter-stability of Au/Al_2O_3 catalysts.[20−22,46] It can be observed in Figure 4a that gold catalyst Au-(Al_2O_3-1)-700 shows excellent activity with a complete CO conversion at 30 °C ($T_{100\%}$ = 30 °C). As shown in Figure 2b, the average diameters of the Au particles are still in the range 2 ± 0.8 nm. On increasing the annealing temperature to 900 °C, the majority of Au particles maintain their small size and are tightly inlayed in the Au-(Al_2O_3-1)-900 through epitaxial growth. Taking one part of an alumina sheet from a whole star-shaped catalyst as one unit marked in Figure 2e, it is estimated that there are ~29 Au nanoparticles with sizes < 5 nm and three particles with sizes > 5 nm. A further rough estimation shows over 1397 Au nanoparticles smaller than <5 nm per μm^2. Au nanoparticles with sizes < 5 nm are necessary for catalytic CO oxidation ($T_{50\%}$ = 158 °C). Compared with the CO conversion of Au-(Al_2O_3-1)-700, the decrease of catalytic performance for Au-(Al_2O_3-1)-900 could be attributed to the encapsulation of active Au sites, as evidenced in Figure 2g and Figure S5. In addition, the N_2 sorption isotherms and textural parameters of gold catalysts Au-(Al_2O_3-1)-700 and Au-(Al_2O_3-1)-900 are provided in Figure S6 and Table S1. The Au-(Al_2O_3-1)-700 sample exhibits a higher specific surface area (173 m^2 g^{-1}) and total pore volume (0.649 cm^3 g^{-1}) than that of Au-(Al_2O_3-1)-900 (105 m^2 g^{-1} and 0.426 cm^3 g^{-1}, accordingly).

For comparison, the Al_2O_3 support was prepared using Na_2CO_3 as the precipitation agent, which was characterized using SEM, XRD, and N_2 adsorption techniques (Figure S7). The SEM image reveals that the obtained alumina is composed of irregular particles, which is significantly different from the alumina prepared using lysine and urea. The prepared Au/Al_2O_3 catalysts calcined at 700 and 900 °C are generally inactive (Figure S7d). The results in turn reveal that such thin porous alumina sheets can efficiently prevent Au nanoparticles against sintering. Supported Au catalysts are typically calcined below 300 °C to retain a small Au particle size and thus activity. Among the nonreducible oxides, gold catalysts supported on Al_2O_3 are intrinsically less active.[40] For example, Au/Al_2O_3 nanofiber catalysts reach a complete CO conversion at 40 °C after annealing in air at 200 °C for 1 h.[48] By comparison, our catalyst Au-(Al_2O_3-1)-250 calcined at 250 °C in air would achieve a complete conversion of CO at ~2 °C (Table 1), and the

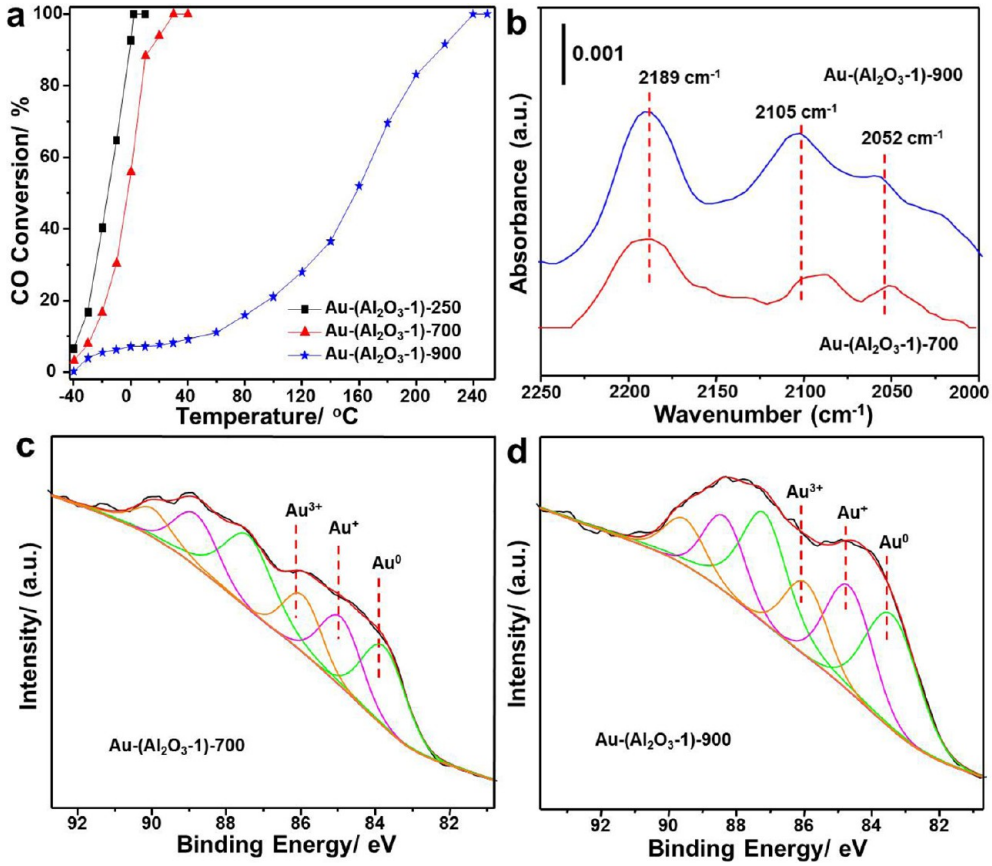

Figure 4. (a) Catalytic activities of gold catalysts Au-(Al_2O_3-1)-250, Au-(Al_2O_3-1)-700, and Au-(Al_2O_3-1)-900. (b) *In situ* DRIFTS and (c, d) Au 4f XPS spectra of the gold catalysts Au-(Al_2O_3-1)-700 and Au-(Al_2O_3-1)-900.

TABLE 1. Dispersion, Catalytic Activity, and XPS Results of the Gold Catalysts

							XPS Au_{4f} peak		
sample	Au dispersion[a] (%)	Au content[b] (wt %)	$T_{100\%}$ (°C)	X_{CO}[b] (%)	rate[b] (mol h^{-1} g_{Au}^{-1})	TOF[b,c] (s^{-1})	Au^0 (atom %)	Au^+ (atom %)	Au^{3+} (atom %)
Au-(Al_2O_3-1)-250	55.6	2.4	2	94	1.433	0.141	56.5	43.5	
Au-(Al_2O_3-1)-700	45.5	2.3	30	56	0.922	0.111	47.2	30.7	22.1
Au-(Al_2O_3-1)-900	40.0	2.7	240	8	0.106	0.015	48.8	31.1	20.1

[a] The dispersion of Au nanoparticles was estimated using the equation $D = 0.9/d_{Au}$.[47] Among them, the size distribution (d_{Au}) comes from the corresponding TEM observation. [b] The actual Au content was detected by ICP technique. The values of CO conversion (X_{CO}), rate, and TOF were estimated at 0 °C. $T_{100\%}$ represents the temperature of 100% CO conversion. [c] Turnover frequency (TOF) was calculated based on the number of supported Au atoms.

corresponding Au nanoparticles are very well-distributed with an average diameter of ~1.8 nm (Figure S8). Concerning the stability of Au catalysts, we have tested the stability of one representative catalyst, Au-(Al_2O_3-1)-250. A good stability at reaction atmosphere during a few hours and under different space rates can be observed in Figure S9. A comparative summary of the recent literature is listed in Table S2 and supports the extraordinary activity of our Au catalyst described here.

To further explore the surface chemical properties of the gold on Al_2O_3 support under high annealing temperatures (700 and 900 °C), *in situ* diffuse reflectance infrared Fourier transform spectroscopy (DRIFTS) was used to measure the adsorbed CO. As shown in Figure 4b, a strong band at 2189 cm^{-1} was attributed to CO adsorbed on cationic gold (Au(I) or Au(III)).[35] The peaks at 2105 and 2052 cm^{-1} belong to two linear CO species adsorbed on the metallic Au sites.[49] The DRIFTS measurements show the presence of $Au^{\delta+}$ and Au^0 on the surface of Au/Al_2O_3 catalysts calcined at 700 and 900 °C, which is consistent with the results of XPS (Figure 4c,d). Compared with the Au catalysts calcined at 250 °C, the amount of $Au^{\delta+}$ species increased with an increasing annealing temperature (Table 1). Furthermore, to understand the character of gold particles dispersed on the thin sheet alumina support, Au/Al_2O_3 catalysts were pretreated at 250 °C under both a hydrogen and oxygen atmosphere. It can be

seen in Figure S10 and Table S3 that both Au^0 and $Au^{\delta+}$ exist on the surface of gold catalysts after redox treatment with hydrogen and oxygen, although stronger absorption bands of Au^0-CO were observed.

^{27}Al MAS NMR spectroscopy has been used to analyze the aluminum cations. Spectra for the γ-Al_2O_3 support and the Au/Al_2O_3 samples annealed at 700 and 900 °C are shown in Figure S11a. Two characteristic peaks centered at 9 and 69 ppm represent the Al^{3+} ions in hexahedral and tetrahedral coordination, respectively, while the 35 ppm NMR peak assigned to the pentacoordinate site has not detected.[50] This suggests that Al predominantly existed in octahedral and tetrahedral sites in our work. To further investigate the interactions between Au nanoparticles and alumina supports, extended X-ray absorption fine structure (EXAFS) was used on Au-(Al_2O_3-1)-700 before and after CO oxidation, as shown in Figure S11b. The peak at 1.2−1.4 Å is associated with Au−O scattering in an oxidized species, and two dominant peaks attributed to Au−Au scattering emerged at 2.4−3.0 Å.[51] This shows the presence of Au^0 and $Au^{\delta+}$ following annealing at 700 °C. The fitted parameters of Au particles—coordination number (*N*), bond distance (*R*), and Debye−Waller factor (or bond disorder)—are all listed in Table S4. The derived structural parameters of particle size and Au dispersion are also included. Using the coordination number (*N*) and bond distance (*R*) values,[52,53] the size of Au particles after CO oxidation was calculated as *ca.* 3.6 ± 2.7 nm for Au-(Al_2O_3-1)-700.

CONCLUSION

Thin porous alumina sheets with an open structure and rough surface have been synthesized *via* a lysine-assisted hydrothermal approach. The architecture of the alumina support and strong interfacial interactions are responsible for stabilizing Au nanoparticles at high temperatures. TEM observation reveals a good lattice match between Al_2O_3 and Au in corresponding crystal planes, identifying that gold nanoparticles are epitaxially grown into the unique alumina supports, and an interfacial restructuring leads to encapsulation of Au particles at an annealing temperature of 900 °C. As a typical and size-dependent reaction, CO oxidation is used to evaluate the performance of Au/Al_2O_3 catalysts. An extraordinary stability and excellent catalytic activity can be achieved, which further confirms the small size and high dispersion of Au nanoparticles. Thus, this finding reveals that such thin porous alumina sheets can stabilize Au nanoparticles against sintering through the SMSI, and such materials could also be excellent supports for other metal nanocatalysts.

METHODS

Synthesis of Thin Porous Aluminum Oxide Sheets. The typical procedure to synthesize thin porous alumina sheets is as follows: 0.75 g of $Al(NO_3)_3 \cdot 9H_2O$, 0.296 g of lysine, and 0.961 g of $CO(NH_2)_2$ (all powders) were dissolved in deionized water to form a homogeneous solution (100 mL) under magnetic stirring for 10 min. Then the solution with a pH of ~4 was transferred into a 150 mL Teflon-lined stainless autoclave and maintained at 100 °C for 24 h. The pH of the reaction solution after hydrothermal synthesis is approximately 8−9. After air-cooling to room temperature, the white precipitate was filtered and washed with deionized water and anhydrous alcohol several times and then dried in a vacuum oven at 80 °C for 12 h. This has been denoted as Al_2O_3-1-hydro. Finally, the γ-Al_2O_3 was obtained by calcination of the powder in air at 500 °C for 2 h with a heating rate of 1 °C min^{-1}. The final product was denoted as Al_2O_3-1. Alumina prepared by $Al(NO_3)_3 \cdot 9H_2O$ and Na_2CO_3 was named as Al_2O_3-2.

Preparation of Au/Al_2O_3 Catalyst. Using 500 °C calcined γ-Al_2O_3 as the catalyst support, Au/Al_2O_3 catalysts were prepared by a deposition−precipitation method using an $HAuCl_4$ solution of pH 8−9 (adjusted by a 0.5 M $(NH_4)_2CO_3$ solution) at 60 °C for 2 h. The product was then washed three times with deionized water and once with alcohol followed by centrifugal separation and drying under vacuum. Finally, the powder was annealed under a flow of air at various temperatures (250, 700, and 900 °C) for 2 h. The obtained Au catalyst was named as Au-(Al_2O_3-1)-*x*, where *x* represents the annealing temperature of the gold catalyst. For instance, gold catalyst supported on Al_2O_3-1 and calcined at 900 °C has been denoted as Au-(Al_2O_3-1)-900. The Au content of a supported catalyst was calculated to be 3 wt %. The actual Au content was detected by the ICP technique.

Catalytic Test. The catalytic activity of Au/Al_2O_3 in CO oxidation was tested in a fixed bed quartz reactor using 50 mg of catalyst. The total flow rate of the reaction gas was 67 mL min^{-1} with a composition of 1 vol % CO, 20 vol % O_2, and 79 vol % N_2, corresponding to a space velocity of 80 000 mL h^{-1} g_{cat}^{-1}. The products were analyzed using a GC-7890 gas chromatograph equipped with a thermal conductivity detector. All the catalysts were tested in the first run.

Characterization. Thermogravimetric and differential scanning calorimetry analysis (TG-DSC) were conducted on a thermogravimetric analyzer STA 449 F3 (NETZSCH), under an air atmosphere with a heating rate of 10 °C min^{-1}. TG-MS was performed on a NETZSCH STA 449 F3 thermobalance coupled with an OmniStar GSD 320 mass spectrometer with a heating rate of 10 °C min^{-1}. X-ray diffraction (XRD) patterns were obtained with a D/MAX-2400 diffractometer using Cu Kα radiation (40 kV, 100 mA, λ = 1.54056 Å). Nitrogen adsorption/desorption isotherms were measured with a TriStar 3000 adsorption analyzer (Micromeritics) at 77 K. The samples were degassed at 473 K for 4 h prior to analysis. The Brunauer−Emmett−Teller (BET) method was utilized to calculate the specific surface areas (S_{BET}). Infrared Fourier transform spectra (FT-IR) were recorded using a Nicolet 6700 FT-IR spectrometer at a resolution of 4 cm^{-1} over the range 4000−640 cm^{-1}. Transmission electron microscope (TEM) images were obtained with a Tecnai $G^2$20 S-Twin microscope with an accelerative voltage of 200 kV. HAADF-STEM images were obtained on a JEOL2010F instrument using an electron probe (0.5 nm diameter) at a diffraction camera length of 10 cm. Scanning electron microscope (SEM) images were obtained from a Hitachi S-4800 instrument. All EXAFS spectra were collected in transmission mode. Powder samples were pressed into pellets with optimal thickness to ensure good-quality data. X-ray intensities before and after sample evaluation were measured using ionization chambers filled with N_2. In addition, a reference spectrum of Au foil for energy calibration was collected simultaneously with each scan using an additional ionization chamber. EXAFS oscillations were extracted using Athena, and fitting of EXAFS data was performed using Artemis[54] and scattering paths generated by the FEFF code (version 6.0).[55] The fitting was limited to 2.0−16.0 $Å^{-1}$ using a Hanning window

with dk = 1.0 Å^{-1}. The fits were performed to both the real and imaginary parts of $\chi(R)$ in the region of $1.0 < R < 3.5$ Å. Similar analysis was performed on the Au foil to obtain S_0^2, the amplitude reduction factor, for the subsequent determination of the coordination numbers of the fitted structure of the samples. Infrared Fourier transform spectra (FT-IR) were recorded using a Nicolet 6700 FT-IR spectrometer at a resolution of 4 cm^{-1} and scale at 4000−640 cm^{-1}. *In situ* diffuse reflectance infrared Fourier transform spectra were recorded using a Nicolet 6700 FT-IR spectrometer at a resolution of 4 cm^{-1} and scale of 4000−640 cm^{-1}. Self-supporting disks were prepared from the sample powders and treated directly in the IR cell. The catalysts were connected to a vacuum-adsorption apparatus with a residual pressure below 10^{-3} Pa. Prior to CO adsorption (5 vol % CO and N_2 in balance), the catalysts were evacuated for 30 min at 200 °C. After flushing with pure He for 10 min, the CO spectrum was collected again. Elemental analysis was carried out on an elemental analyzer (Vario EL III, Elementar). ^{27}Al MAS NMR spectra were recorded on a Bruker AVANCE III-600 spectrometer with a 2.5 mm MAS probe at 156.4 MHz with a spinning rate of 30 kHz, 200 scans, and 2 s recycle delay. The chemical shifts were referenced to the 1% $Al(NO_3)_3$ aqueous solution. X-ray photoelectron spectroscopy (XPS) studies were performed using monochromatic Al Kα radiation (ESCALAB250, thermo VG), and the binding energies of samples were calibrated by taking the carbon 1s peak as reference (284.6 eV). The actual gold content was analyzed using an inductively coupled plasma atomic emission spectrometer (ICP-AES) on the Optima 2000 DV.

Conflict of Interest: The authors declare no competing financial interest.

Acknowledgment. The project was supported by the National Natural Science Foundation of China (No. 20973031) and the Ph.D. Programs Foundation (20100041110017) of Ministry of Education of China.

Supporting Information Available: The results of XRD, SEM, TEM, FTIR, XPS, EXAFS, ^{27}Al MAS NMR, and catalytic performance are provided as Supporting Information. This material is available free of charge *via* the Internet at http://pubs.acs.org.

REFERENCES AND NOTES

1. Zou, X. H.; Qi, S. X.; Suo, Z. H.; An, L. D.; Li, F. Activity and Deactivation of Au/Al_2O_3 Catalyst for Low-Temperature CO Oxidation. *Catal. Commun.* **2007**, *8*, 784–788.
2. Konova, P.; Naydenov, A.; Venkov, C.; Mehandjiev, D.; Andreeva, D.; Tabakova, T. Activity and Deactivation of Au/TiO_2 Catalyst in CO Oxidation. *J. Mol. Catal. A* **2004**, *213*, 235–240.
3. Konova, P.; Naydenov, A.; Tabakova, T.; Mehandjiev, D. Deactivation of Nanosize Gold Supported on Zirconia in CO Oxidation. *Catal. Commun.* **2004**, *5*, 537–542.
4. Haruta, M. Catalysis of Gold Nanoparticles Deposited on Metal Oxides. *CATECH* **2002**, *6*, 102–115.
5. Chiang, C.-W.; Wang, A.-Q.; Mou, C.-Y. CO Oxidation Catalyzed by Gold Nanoparticles Confined in Mesoporous Aluminosilicate Al-SBA-15: Pretreatment Methods. *Catal. Today* **2006**, *117*, 220–227.
6. Bandyopadhyay, M.; Korsak, O.; van den Berg, M. W. E.; Grünert, W.; Birkner, A.; Li, W.-C.; Schüth, F.; Gies, H. Gold Nano-Particles Stabilized in Mesoporous MCM-48 as Active CO-Oxidation Catalyst. *Microporous Mesoporous Mater.* **2006**, *89*, 158–163.
7. Gabaldon, J. P.; Bore, M.; Datye, A. K. Mesoporous Silica Supports for Improved Thermal Stability in Supported Au Catalysts. *Top. Catal.* **2007**, *44*, 253–262.
8. Sun, J.-M.; Ma, D.; Zhang, H.; Liu, X.-M.; Han, X.-W.; Bao, X.-H.; Weinberg, G.; Pfänder, N.; Su, D.-S. Toward Monodispersed Silver Nanoparticles with Unusual Thermal Stability. *J. Am. Chem. Soc.* **2006**, *128*, 15756–15764.
9. Chen, W.; Fan, Z.-L.; Pan, X.-L.; Bao, X.-H. Effect of Confinement in Carbon Nanotubes on the Activity of Fischer−Tropsch Iron Catalyst. *J. Am. Chem. Soc.* **2008**, *130*, 9414–9419.
10. Arnal, P. M.; Comotti, M.; Schüth, F. High-Temperature-Stable Catalysts by Hollow Sphere Encapsulation. *Angew. Chem., Int. Ed.* **2006**, *45*, 8224–8227.
11. Lee, I.; Joo, J. B.; Yin, Y.; Zaera, F. A Yolk@Shell Nanoarchitecture for Au/TiO_2 Catalysts. *Angew. Chem., Int. Ed.* **2011**, *50*, 10208–10211.
12. Lee, J.; Park, J. C.; Song, H. A Nanoreactor Framework of a Au@SiO_2 Yolk/Shell Structure for Catalytic Reductuon of p-Nitrophenol. *Adv. Mater.* **2008**, *20*, 1523–1528.
13. Yu, K.; Wu, Z.-C.; Zhao, R.-Q.; Li, B.-X.; Xie, Y. High-Temperature-Stable Au@SnO_2 Core/Shell Supported Catalyst for CO Oxidation. *J. Phys. Chem. C* **2008**, *1123*, 2244–2247.
14. Joo, S. H.; Park, J. Y.; Tsung, C. K.; Yamada, Y.; Yang, P. D.; Somorjai, G. A. Thermally Stable Pt/Mesoporous Silica Core-Shell Nanocatalysts for High-Temperature Reactions. *Nat. Mater.* **2009**, *8*, 126–131.
15. Ikeda, S.; Ishino, S.; Haranda, T.; Okamoto, N.; Sakata, T.; Mori, H.; Kuwabata, S.; Torimoto, T.; Matsumura, M. Ligand-Free Platinum Nanoparticles Encapsulated in a Hollow Porous Carbon Shell as a Highly Active Heterogeneous Hydrogenation Catalyst. *Angew. Chem., Int. Ed.* **2006**, *45*, 7063–7066.
16. Yin, Y.; Rioux, R. M.; Erdonmez, C. K.; Hughes, S.; Somorjai, G. A.; Alivisatos, A. P. Formation of Hollow Nanocrystals through the Nanoscale Kirkendall Effect. *Science* **2004**, *304*, 711–714.
17. Yuan, Q.; Yin, A.-X.; Luo, C.; Sun, L.-D.; Zhang, Y.-W.; Duan, W.-T.; Liu, H.-C.; Yan, C.-H. Facile Synthesis for Ordered Mesoporous γ-Aluminas with High Thermal Stability. *J. Am. Chem. Soc.* **2008**, *130*, 3465–3472.
18. Liu, Q.; Wang, A.-Q.; Xu, J.-M.; Zhang, Y.-H.; Wang, X.-D.; Zhang, T. Preparation of Ordered Mesoporous Crystalline Alumina Replicated by Mesoporous Carbon. *Microporous Mesoporous Mater.* **2008**, *116*, 461–468.
19. Li, W.-C.; Lu, A.-H.; Weidenthaler, C.; Goddard, R.; Bongard, H. J.; Schüth, F. Growth of Single Crystal α-Al_2O_3 Nanofibers on a Carbon Aerogel Substrate. *J. Mater. Chem.* **2005**, *15*, 2993–2996.
20. Bond, G. C.; Thompson, D. T. Gold-Catalysed Oxidation of Carbon Monoxide. *Gold Bull.* **2000**, *33*, 41–50.
21. Wen, L.; Fu, J.-K.; Gu, P.-Y.; Yao, B.-X.; Lin, Z.-H.; Zhou, J.-Z. Monodispersed Gold Nanoparticles Supported on γ-Al_2O_3 for Enhancement of Low-Temperature Catalytic Oxidation of CO. *Appl. Catal., B* **2008**, *79*, 402–409.
22. Haruta, M.; Daté, M. Advance in the Catalysis of Au Nanoparticles. *Appl. Catal., A* **2001**, *222*, 427–437.
23. Wang, G.-H.; Li, W.-C.; Jia, K.-M.; Spliethoff, B.; Schüth, F.; Lu, A.-H. Shape and Size Controlled α-Fe_2O_3 Nanoparticles as Supports for Gold-Catalysts: Synthesis and Influence of Support Shape and Size on Catalytic Performance. *Appl. Catal., A* **2009**, *364*, 42–47.
24. Hao, G.-P.; Li, W.-C.; Wang, S.; Wang, G.-H.; Qi, L.; Lu, A.-H. Lysine-Assisted Rapid Synthesis of Crack-Free Hierarchical Carbon Monoliths with a Hexagonal Array of Mesopores. *Carbon* **2011**, *49*, 3762–3772.
25. Hao, G.-P.; Li, W.-C.; Qian, D.; Lu, A.-H. Rapid Synthesis of Nitrogen-Doped Porous Carbon Monolith for CO_2 Capture. *Adv. Mater.* **2010**, *22*, 853–857.
26. Dong, Y.-R.; Nishiyama, N.; Egashira, Y.; Ueyama, K. Basic Amid Acid-Assisted Synthesis of Resorcinol-Formaldehyde Polymer and Carbon Nanospheres. *Ind. Eng. Chem. Res.* **2008**, *47*, 4712–4716.
27. Yokoi, T.; Sakamoto, Y.; Terasaki, O.; Kubota, Y.; Okubo, T.; Tatsumi, T. Periodic Arrangement of Silica Nanospheres Assisted by Amino Acids. *J. Am. Chem. Soc.* **2006**, *128*, 13664–13665.
28. Ram, S.; Rana, S. Synthesis of Mesoporous Clusters of $AlO(OH)\cdot\alpha H_2O$ by a Surface Hydrolysis Reaction of Pure Al-Metal with Nascent-Surface in Water. *Mater. Lett.* **2000**, *42*, 52–60.
29. Kim, J. H.; Jung, K. Y.; Park, K. Y.; Cho, S. B. Characterization of Mesoporous Alumina Particles Prepared by Spray Pyrolysis of $Al(NO_3)\cdot 9H_2O$ Precursor: Effect of CTAB and Urea. *Microporous Mesoporous Mater.* **2010**, *128*, 85–90.

30. Roiban, L.; Sorbier, L.; Pichon, C.; Pham-Huu, C.; Drillon, M.; Ersen, O. 3D-TEM Investigation of the Nanostructure of a δ-Al_2O_3 Catalyst Support Decorated with Pd Nanoparticles. *Nanoscale* **2012**, *4*, 946–954.
31. Zhu, Z.; Sun, H.; Liu, H.; Yang, D. PEG-Directed Hydrothermal Synthesis of Alumina Nanorods with Mesoporous Structure *via* AACH Nanorod Precursors. *J. Mater. Sci.* **2010**, *45*, 46–50.
32. Feng, Y.; Lu, W.; Zhang, L.; Bao, X.; Yue, B.; Iv, Y.; Shang, X. One-Step Synthesis of Hierarchical Cantaloupe-Like AlOOH Superstructures via a Hydrothermal Route. *Cryst. Growth Des.* **2008**, *8*, 1426–1429.
33. Zhang, L.; Jiao, X.; Chen, D.; Jiao, M. γ-AlOOH Nanomaterials with Regular Shapes: Hydrothermal Fabrication and $Cr_2O_7^{2-}$ Adsorption. *Eur. J. Inorg. Chem.* **2011**, 5258–5264.
34. Turek, A. M.; Wachs, I. E. Acidic Properties of Alumina-Supported Metal Oxide Catalysts: An Infrared Spectroscopy Study. *J. Phys. Chem.* **1992**, *96*, 5000–5007.
35. Parkyns, N. D. Influence of Thermal Pretreatment on the Infrared Spectrum of Carbon Dioxide Adsorbed on Alumina. *J. Phys. Chem.* **1971**, *75*, 526–531.
36. Wijnja, H.; Schulthess, C. P. ATR-FTIR and DRIFT Spectroscopy of Carbonate Species at the Aged γ-Al_2O_3/Water Interface. *Spectrochim. Acta, Part A* **1999**, *55*, 861–872.
37. Shen, S. C.; Chen, Q.; Chow, P. S.; Tan, G. H.; Zeng, X. T.; Wang, Z.; Tan, R. B. H. Steam-Assisted Solid Wet-Gel Synthesis of High-Quality Nanorods of Boehmite and Alumina. *J. Phys. Chem. C* **2007**, *111*, 700–707.
38. Cruz, A. M. D.; Eon, J. G. Boehmite-Supported Vanadium Oxide Catalysts. *Appl. Catal., A* **1998**, *167*, 203–213.
39. Nanda, K. K.; Sahu, S. N.; Behera, S. N. Liquid-Drop Model for the Size-Dependent Melting of Low-Dimensional Systems. *Phys. Rev. A* **2002**, *66*, 013208–013216.
40. Schubert, M. M.; Hackenberg, S.; van Veen, A. C.; Muhler, M.; Plzak, V.; Behm, R. J. CO Oxidation over Supported Gold Catalysts—"Inert" and "Active" Support Materials and Their Role for the Oxygen Supply during Reaction. *J. Catal.* **2001**, *197*, 113–122.
41. Liu, X.; Liu, M.-H.; Luo, Y.-C.; Mou, C.-Y.; Lin, S. D.; Cheng, H.; Chen, J.-M.; Lee, J.-F.; Lin, T.-S. Strong Metal-Support Interactions between Gold Nanoparticles and ZnO Nanorods in CO Oxidation. *J. Am. Chem. Soc.* **2012**, *134*, 10251–10258.
42. Somorjai, G. A.; Park, J. Y. Molecular Facters of Catalytic Selectivity. *Angew. Chem., Int. Ed.* **2008**, *47*, 9212–9228.
43. Lu, W. G.; Ding, Y.; Chen, Y. X.; Wang, Z. L.; Fang, J. Y. Bismuth Telluride Hexagonal Nanoplatelets and Their Two-Step Epitaxial Growth. *J. Am. Chem. Soc.* **2005**, *127*, 10112–10116.
44. Fan, F.-R.; Ding, Y.; Liu, D.-Y.; Tian, Z.-Q.; Wang, Z. L. Facet-Selective Epitaxial Growth of Heterogeneous Nanostructures of Semiconductor and Metal: ZnO Nanorods on Ag Nanocrystals. *J. Am. Chem. Soc.* **2009**, *131*, 12036–12037.
45. Murthy, V. S. R.; Jena, A. K.; Gupta, K. P.; Murty, G. S. *Structure and Properties of Engineering Materials*; Tata McGraw-Hill Pub. Co., 2003; pp 98—99.
46. Xie, X.; Li, Y.; Liu, Z.-Q.; Haruta, M.; Shen, W. J. Low-Temperature Oxidation of CO Catalysed by Co_3O_4 Nanorods. *Nature* **2009**, *458*, 746–749.
47. Cai, W. J.; Wang, F. G.; Daniel, C.; van Veen, A. C.; Schuurman, Y.; Descorme, C.; Provendier, H.; Shen, W. J.; Mirodatos, C. Oxidation of Steam Reforming of Ethanol over Ir/CeO_2 Catalysts: A Structure Sensitivity Analysis. *J. Catal.* **2012**, *286*, 137–152.
48. Han, Y.-F.; Zhong, Z.; Ramesh, K.; Chen, F.; Chen, L. Effects of Different Types of γ-Al_2O_3 on the Activity of Gold Nanoparticles for CO Oxidation at Low-Temperatures. *J. Phys. Chem. C* **2007**, *111*, 3163–3170.
49. Roze, E.; Gravejat, P.; Quinet, E.; Rousset, J. L.; Bianchi, D. Impact of the Reconstruction of Gold Particles on the Heats of Adsorption of Linear CO Species Adsorbed on the Au Sites of a 1% Au/Al_2O_3 Catalyst. *J. Phys. Chem. C* **2009**, *113*, 1037–1045.
50. Kwak, J. H.; Hu, J. Z.; Mei, D. H.; Yi, C.-W.; Kim, D. H.; Peden, C. H. F.; Allard, L. F.; Szanyi, J. Coordinatively Unsaturated Al^{3+} Centers as Binding Sites for Active Catalyst Phases of Platinum on γ-Al_2O_3. *Science* **2009**, *325*, 1670–1673.
51. Delannoy, L.; Weiher, N.; Nikolaos, T.; Beesley, A. M.; Nchari, L.; Schroeder, S. L. M.; Louis, C. Reducibility of Supported Gold (III) Precursors: Influence of the Metal Oxide Support and Consequences for CO Oxidation Activity. *Top. Catal.* **2007**, *44*, 263–273.
52. Miller, J. T.; Kropf, A. J.; Zha, Y.; Regalbuto, J. R.; Delannoy, L.; Louis, C.; Bus, E.; van Bokhoven, J. A. The Effect of Gold Particles Size on Au-Au Bond Length and Reactivity towards Oxygen in Supported Catalysts. *J. Catal.* **2006**, *240*, 222–234.
53. Calvin, S.; Miller, M. M.; Goswami, R.; Cheng, S.-F.; Mulvaney, S. P.; Whitman, L. J.; Harris, V. G. Determination of Crystallite Size in a Magnetic Nanocomposite using Extended X-Ray Absorption Fine Structure. *J. Appl. Phys.* **2003**, *94*, 778–783.
54. Ravel, B.; Newville, M. ATHENA, ARTEMIS, HEPHAESTUS: Data Analysis for X-Ray Absorption Spectroscopy using IFEFFIT. *J. Synchrotron Rad.* **2005**, *12*, 537–541.
55. Newville, M. EXAFS Analysis using FEFF and FEFFIT. *J. Synchrotron Rad.* **2001**, *8*, 96–100.